Available online at www.sciencedirect.com
ScienceDirect
Journal of Computational Physics 227 (2008) 7222–7245
JOURNAL OF COMPUTATIONAL PHYSICS
www.elsevier.com/locate/jcp

A PIC-MCC code for simulation of streamer propagation in air

O. Chanrion *, T. Neubert

DTU Space, National Space Institute, Technical University of Denmark, Juliane Maries Vej 30, DK-2100 Copenhagen, Denmark

Received 24 March 2007; received in revised form 8 April 2008; accepted 8 April 2008
Available online 30 April 2008

Abstract

A particle code has been developed to study the distribution and acceleration of electrons in electric discharges in air. The code can follow the evolution of a discharge from the initial stage of a single free electron in a background electric field to the formation of an electron avalanche and its transition into a streamer. The code is in 2D axi-symmetric coordinates, allowing quasi 3D simulations during the initial stages of streamer formation. This is important for realistic simulations of problems where space charge fields are essential such as in streamer formation. The charged particles are followed in a Cartesian mesh and the electric field is updated with Poisson's equation from the charged particle densities. Collisional processes between electrons and air molecules are simulated with a Monte Carlo technique, according to cross section probabilities. The code also includes photoionisation processes of air molecules by photons emitted by excited constituents. The paper describes the code and presents some results of streamer development at 70 km altitude in the mesosphere where electrical discharges (sprites) are generated above severe thunderstorms and at ~10 km relevant for lightning and thundercloud electrification. The code is used to study acceleration of thermal seed electrons in streamers and to understand the conditions under which electrons may reach energies in the runaway regime. This is the first study in air, with a particle model with realistic spatial dependencies of the electrostatic field. It is shown that at 1 atm pressure the electric field must exceed ~7.5 times the breakdown field to observe runaway electrons in a constant electric field. This value is close to the field where the electric force on an electron equals the maximum frictional force on an electron – found at ~100 eV. It is also found that this value is reached in a negative streamer tip at 10 km altitude when the background electric field equals ~3 times the breakdown field. At higher altitudes, the background electric field must be relatively larger to create a similar field in a streamer tip because of increased influence of photoionisation. It is shown that the role of photoionization increases with altitude and the effect is to decrease the space charge fields and increase the streamer propagation velocity. Finally, effects of electrons in the runaway regime on negative streamer dynamics are presented. It is shown the energetic electrons create enhanced ionization in front of negative streamers. The simulations suggest that the thermal runaway mechanism may operate at lower altitudes and be associated with lightning and thundercloud electrification while the mechanism is unlikely to be important in sprite generation at higher altitudes in the mesosphere.

PACS: 97.10.Gz; 97.30.Qt; 97.80.Gm

Keywords: PIC-MCC; Streamer; Discharge; Sprite

* Corresponding author.
E-mail address: chanrion@space.dtu.dk (O. Chanrion).

0021-9991/$ - see front matter © 2008 Elsevier Inc. All rights reserved.
doi:10.1016/j.jcp.2008.04.016

1. Introduction

Sprites are transient luminous flashes in the mesosphere at 50–90 km altitude above large thunderstorms [1]. Sprites are usually associated with positive cloud-to-ground lightning discharges (+CG) [2,3]. They are electric discharges driven by the electric field in the mesosphere, established by the impulsive adjustments of the charge configuration in the thundercloud below. Telescopic imaging has shown vertical filamentous structures of sprites with diameters of 100 m or less [4–6], interpreted as streamers [7–9]. Streamers are filaments of ionised air that can initiate from an electron avalanche when the electric field exceeds the threshold for breakdown [10]. They occur when the space charge of the avalanche reaches a magnitude comparable to the background electric field. Negative streamers propagate in the direction against the electric field (in the direction of electron acceleration) and positive streamers along the field. Positive streamers require the presence of seed electrons from background ionisation or photoionisation.

It has been suggested [11] that streamers may be a contributing source of X- and γ-ray emissions observed from spacecraft above thunderstorms, the so-called terrestrial γ-ray flashes (TGF) [12]. TGFs are thought to be bremsstrahlung from energetic (MeV) electrons accelerated in the atmosphere by thunderstorm electric fields. X- and γ-radiation is also observed in relation to normal cloud-to-ground (CG) lightning [13,43], within thunderstorms [14], and in laboratory discharges [15]. The realisation that energetic electrons can be an integral part of electrical discharges is fairly recent. Since most simulation tools developed for studies of streamer discharges are based on the fluid approach, they are not well suited to study the problem. For this reason a particle code has been developed which allows for self-consistent calculation of the space charge fields and the acceleration of electrons. The code is described in Section 2, and the validation of the code in Section 3, where some results on streamer formation and propagation are compared with those of fluid models [16]. Section 4 contains a study on electron acceleration in streamers for different level of photoionisation. Section 5 contains the conclusions.

2. The simulation code

2.1. The physical model

The model assumes cylinder symmetry and is given in cylindrical coordinates with the z-axis along the background electric field. We consider a flow of electrons traveling through the atmosphere under the action of the field. The electrons interact with the neutral gas through elastic and inelastic collisions that ionise and excite atmospheric constituents and via attachment. The model describes the evolution in time of electrons and their interactions with the atmospheric constituents. Ions are considered immobile on the short time scales considered and are stationary at their location of creation. The neutral gas is considered weakly ionised such that perturbations to the gas density and temperature are ignored. The electric charge and currents generated in the discharge radiate electromagnetic fields. In the simulations we consider only the electric field and neglect the action of a background magnetic field and induction fields. The electric field is then the main source of non-linearity in the model.

The distribution function of the charged particle species is described mathematically by the Vlasov–Boltzmann equation [17]:

$$\begin{aligned}
&\frac{\partial f_e}{\partial t} + {}_r\nabla_r f_e + {}_{,}\nabla_{,} f_e + \frac{{}^2_{\theta}}{r}\nabla {}_r f_e - \frac{{}_r {}_{\theta}}{r}\nabla {}_{\theta} f_e \\
&\quad - \frac{eE_r}{m_e}\nabla {}_r f_e - \frac{eE_{,}}{m_e}\nabla {}_{,} f_e = Q_e(f_e) \\
&\frac{\partial f_i}{\partial t} = Q_i(f_e)
\end{aligned} \tag{1}$$

Here e is the elementary charge, m_e is the mass of an electron, $\vec{}$ its speed and f_α the distribution function of species α ('e' for electrons and 'i' for ions). Q_α are the Boltzmann collision terms that account for both elastic and inelastic collisions. In the following the collisions will be described by their differential cross sections:

$\sigma_k(v, \chi, \phi)$. Where the k-index represents the type of collisional process, such as elastic, excitation, attachment or ionisation. The χ and ϕ angles represent respectively the deviation angle and azimuthal angle from the initial velocity $\vec{}$ of magnitude v of a colliding particle.

The electric field consistent with the charge distribution is found from Poisson's equation for the electric potential Φ. In cylindrical coordinates it is given by:

$$-\frac{1}{r}\frac{\partial}{\partial r}\left(r.\frac{\partial}{\partial r}\Phi(r,\ )\right)-\frac{\partial^2}{\partial\ ^2}\Phi(r,\ )=\frac{e}{\epsilon_0}(n_i(r,\ )-n_e(r,\ ))=\frac{e}{\epsilon_0}\rho(r,\ ) \tag{2}$$

where n_α is the density of species α, defined by:

$$n_\alpha(t,r,\ )=\int_{r,\ \theta,\ } f_\alpha(t,r,\ ,\ r,\ \theta,\ ,)\,\mathrm{d}\ _r\,\mathrm{d}\ _\theta\,\mathrm{d}\ \tag{3}$$

The electric field is then found from the potential gradient.

2.2. The numerical code

The numerical approach is a 2D, axi-symmetrical, Particle-in-Cell (PIC), Monte Carlo collision (MCC) code. Much of the presentation in the following on PIC-MCC refers to the works of Birdsall [18] and Nanbu [17]. In a PIC code, particles move freely within a grid, with the fields given at fixed grid points.

The size of the simulation domain is $L_r \times L_z$ with $N_r \times N_z$ grid points at $(\Delta r, \Delta z)$ intervals. As the number of computer particles is limited by computer memory, each computer particle represents many real particles. In terms of the particle distribution function of electrons f_e, the computer particles are defined by the expression:

$$2\pi r f_e(t,r,\ ,\ r,\ \theta,\ ,)=\sum_p\ _p\delta(r-r_p(t))\delta(\ -\ _p(t))\delta(\ _r-\ _{rp}(t))\delta(\ _\theta-\ _{\theta_p}(t))\delta(\ ,-\ ,_p(t)) \tag{4}$$

where r_p, z_p, v_{rp}, $v_{\theta p}$, v_{zp} are the spatial- and velocity components of the computer particles and w_p their weight.

The evolution of the electron distribution function is found numerically by first advancing particles during one incremental time step $\Delta^c t$ under the action of the electric field to an intermediate distribution function f_e^* that is a solution to the collisionless Boltzmann equation (the Vlasov equation), then by adding the contribution of the collisions during that time step to the solution. The magnitude of $\Delta^c t$ in the code is determined by the collisional processes. The self-consistent field is updated by solving the Poisson's equation at time steps Δt which in general are larger than $\Delta^c t$.

To find the distribution f_e^* for an incremental timestep $\Delta^c t$, the distribution function is first transported along the characteristics of the Vlasov equation which are the particle trajectories. Solving the Vlasov equation is then reduced to solving for the particle trajectories. This is done using the standard first order Euler method, which determines the new positions and velocities of the computer particles. In order to avoid errors near the cylinder axis, the scheme has been written in 3D Cartesian coordinates and projected to the 2D-cylindrical ones [19].

2.3. The Monte Carlo collision scheme

Collisions are done with the Monte Carlo scheme from Nanbu [20] that is known to be efficient when the number of different types of colliding processes N_{coll} is large. A first order approximation of the integration of the Boltzmann equation during t and $t+\Delta^c t$ is given by:

$$f_e(t+\Delta^c t)\simeq f_e^*(t+\Delta^c t)+\Delta^c t Q_e(f_e^*(t+\Delta^c t)) \tag{5}$$

Using the particle approximation of the distribution function, approximating this integral corresponds to changing the velocity of a particle p according the probability it has to collide during $\Delta^c t$. For an electron having the velocity v_p and for a small $\Delta^c t$, the probability the electron suffers a kth collision of integrated cross section $\sigma_k(v_p)$ in a neutral gas of density n_n is given by:

$$P_k = 1 - \exp(-n_n \sigma_k(\ _p)\ _p\Delta^c t) \simeq n_n \sigma_k(\ _p)\ _p\Delta^c t \tag{6}$$

The total probability to collide is then:

$$P = n_n \sigma_{\mathrm{tot}}(\ _p)\ _p\Delta^c t \tag{7}$$

where $\sigma_{\mathrm{tot}}(v_p)$ is the sum of all integrated cross sections $\sigma_k(v_p)$.

The probability of a collision can be visualised by considering a line of unit length, divided into N_{coll} segments of equal length, each representing a collisional process. Each segment is further divided into two, with the right segment representing the probability of collision (P_k) and the left the probability of no collisions ($1/N_{\mathrm{coll}} - P_k$). The probabilities P_k to collide are then distributed on the right sides of all k-intervals. To decide if a collision occurs and which collision number the electron suffers, we choose a random number U_1. If U_1 lies in the right part of the kth interval, the electron suffers a kth type of collision. If U_1 lies in one of the left parts of the intervals, the electron does not collide.

One can note that this method induces a constraint on the choice of the time step $\Delta^c t$. Introducing the collision frequency $\gamma_k(v_p) = n_n \sigma_k(v_p) v_p$, we must require that:

$$\Delta^c t < \Delta^c_{\max} t = \frac{1}{N_{\mathrm{coll}} \gamma_{\max}} \tag{8}$$

Where $\gamma_{\max}$ is the maximal collision frequency $\gamma_k(v_p)$ for all velocity v_p and collision processes k considered. Furthermore, with our sets of cross sections, any timestep that fulfills the condition (8) also fulfills the Vahedi and Surendra condition [21]:

$$\forall\ _p, \Delta^c t < \frac{0.1}{\gamma_{\mathrm{tot}}(\ _p)} \tag{9}$$

that allows considering only one collision per time step. Here, $\gamma_{\mathrm{tot}}(v_p) = n_n \sigma_{\mathrm{tot}}(v_p) v_p$ is the total collision frequency.

2.4. The particle energies in the scattering processes

When the type of collision process is determined, if any, the scattering is performed by choosing the velocity after collision. The incident energy of a particle, ϵ_{in}, is shared between the energy consumed in the process ϵ_{co}, the energy of the scattered electron ϵ_{sc} and the energy of the secondary electron ϵ_{ex}, if it is an ionising process. There are three types of collisions considered:

Elastic collisions:

$$\epsilon_{\mathrm{sc}} = \epsilon_{\mathrm{in}} \left(1 - \frac{2m_{\mathrm{e}}}{M}(1 - \cos\chi)\right)$$

In-elastic collisions or excitation:

$$\epsilon_{\mathrm{sc}} = \epsilon_{\mathrm{in}} - \epsilon_{\mathrm{co}}$$

Ionisation:

$$\epsilon_{\mathrm{sc}} = \epsilon_{\mathrm{in}} - \epsilon_{\mathrm{co}} - \epsilon_{\mathrm{ex}}$$

For elastic collisions energy is shared between the electron of mass m_{e} and the air molecule of mass M. For inelastic collisions nitrogen or oxygen atoms are excited to energy levels ϵ_{co}. The code accounts for 48 of the most common collision type (nitrogen: 1 elastic collision, 1 rotational excitation, 9 vibrational excitations, 14 electronic excitations and 3 impact ionisations; oxygen: 1 elastic collision, 1 attachment process, 1 rotational excitation, 6 vibrational excitations, 6 electronic excitations and 5 impact ionisations). The associated scattering process k is determined by the random number U_1. In an ionising collision, the energy is shared between the primary and secondary electron according to Opal et al. [22]:

$$\epsilon_{\mathrm{ex}} = B \tan\left(U_2 \mathrm{atan}\left(\frac{\epsilon_{\mathrm{in}} - \epsilon_{\mathrm{co}}}{2B}\right)\right)$$

where B is a shape parameter chosen to be 15.6 eV for nitrogen and 12.2 eV for oxygen, and U_2 a random number uniformly distributed in the interval [0, 1].

2.5. Cross sections and scattering angles

The cross sections come from the BOLSIG package [23]. The cross sections are extrapolated to high energies up to 100 keV using a first Born approximation [24] for the elastic cross sections and a Born-Bethe approximation [25] for the inelastic cross section.

We consider two models of angular scattering of electron(s). In the first it is assumed that all collisions are isotropic, which is a good assumption for low-energy electrons (eV). In this case, the longitudinal and azimuthal scattering angles (χ, ϕ) can be chosen from a pair of independent random numbers $U_{3,4}$ uniformly distributed in the interval [0, 1] with $\chi = \mathrm{acos}(1 - 2U_3)$ and $\phi = 2\pi\ U_4$. This model is used for validation of the code and for comparison with published work on fluid simulations in Section 3.3.

In the second model the scattering for collision is based on the screened Coulomb potential between electrons and neutral atoms [26]:

$$\sigma_k(\epsilon, \chi, \phi) = \sigma_k(\epsilon)\frac{1}{4\pi}\frac{1 - 2\xi^2(\epsilon)}{(1 - \xi(\epsilon)\cos(\chi))^2} \tag{10}$$

where ξ is a function of the energy ϵ of the electron before the collision given by:

$$\xi(\epsilon) = \frac{0.065\epsilon + 0.26\sqrt{\epsilon}}{1 + 0.05\epsilon + 0.2\sqrt{\epsilon}} - \frac{12\sqrt{\epsilon}}{1 + 40\sqrt{\epsilon}} \tag{11}$$

The scattering angles are here chosen randomly according to

$$\chi = \arccos\left(1 - \frac{2U_3(1 - \xi(\epsilon))}{1 + \xi(\epsilon)(1 - 2U_3)}\right) \quad \text{and} \quad \phi = 2\pi U_4 \tag{12}$$

with U_3 and U_4 two random number uniformly distributed in [0, 1].

For anisotropic scattering, the elastic cross section σ_k needed in our MCC collision model is related to the elastic momentum transfer cross section σ_k^m given in the BOLSIG package [23] by:

$$\sigma_k^m(\epsilon) = \sigma_k(\epsilon)\frac{1 - \xi(\epsilon)}{2\xi^2(\epsilon)}\left((1 + \xi(\epsilon))\ln\left(\frac{1 + \xi(\epsilon)}{1 - \xi(\epsilon)}\right) - 2\xi(\epsilon)\right) \tag{13}$$

This anisotropic model is chosen because it gives good agreement with experimental measurements of both the total elastic cross section and the momentum cross section for N_2 [27,26]. It is used for studies of energetic electrons accelerated in streamers described in Section 4.

2.6. Photoionisation

In order to reproduce the positive streamers in sprites, observed propagating downward in the atmosphere during the action of an assumed downward-directed electric field, it is necessary to reproduce a source of electrons in the region below the positive head. It is assumed that the dominant source is photoionisation rather than background ionisation. The most common assumption on photoionisation in air is that nitrogen is excited by energetic electrons in the streamer tip and that photons emitted by excited nitrogen ionise oxygen in a region surrounding the streamer head. The photoelectrons initiate avalanches that feed the positive streamer head and permit its downward propagation.

We adopt the photoionisation model of Zheleznyak et al. [28], where the emissivity of photons that lead to ionisation of oxygen is assumed to be proportional to the nitrogen ionisation rate. The relative emissivity ψ^* is the number of oxygen photoionisations per impact ionisation:

$$\psi^* = p^*\gamma^*\eta^*$$

where p^* accounts for quenching effects on excited nitrogen, γ^* is the fraction of nitrogen ionisation events that leads to radiation with energy sufficient to ionise oxygen, and η^* the efficiency of those photons to ionise oxygen. The coefficient $\gamma^*\eta^*$ is a function of E/p [28].

To reproduce this proportionality in our particle code, ionising photons are created if a random number $U_p < \psi^*$ for each computer particle that suffers an ionisation event. The number of created photons (N_{ph}) equals the number of electrons the computer particle represents (limited to 10,000). The wave frequency γ of the photons determines their mean free path. It is chosen randomly in the frequency interval $[\gamma_1, \gamma_2]$ able to ionise oxygen using a random number U_γ such that $\gamma = \gamma_1 + U_\gamma(\gamma_2 - \gamma_1)$. ($\gamma_1 = 2.925$ PHz and $\gamma_2 = 3.059$ PHz). The mean free path of the photons before they create an ionisation event of oxygen [16]:

$$K_{\mathrm{f}} = K_1 \left(\frac{K_2}{K_1}\right)^{\frac{\gamma-\gamma_1}{\gamma_2-\gamma_1}} \tag{14}$$

where $K_1 = 3.5P_{\mathrm{O}_2}\ \mathrm{m}^{-1}$ and $K_2 = 200P_{\mathrm{O}_2}\ \mathrm{m}^{-1}$. Thus, for each photon an ion-electron pair is created at a distance d_{ph} chosen with a random number U_{d} such that:

$$d_{\mathrm{ph}} = -K_{\mathrm{f}}^{-1} \ln U_{\mathrm{d}}$$

It is further assumed that the photons are emitted isotropically at angles determined by two random number U_θ and U_ϕ such that:

$$\theta_{\mathrm{ph}} = 2\pi U_\theta$$
$$\phi_{\mathrm{ph}} = \mathrm{acos}(2U_\phi - 1)$$

The ionisation pair will then be created at the position:

$$r_{\mathrm{ph}} = \sqrt{r_p^2 + 2d_p\cos(\theta_p)\sin(\phi_p) + d_p^2\sin^2(\phi_p)}$$
$$\_{\mathrm{ph}} = \__p + d_p\cos(\phi_p)$$

The velocity of the electron and ion is chosen to be null and their weight is given by: $\pm w_p/N_{\mathrm{ph}}$.

The method can be seen as a Monte Carlo approximation of the integral commonly used in fluid simulation given the photoionisation rate [28] at the point X_{ph}:

$$\frac{\partial f^{\mathrm{ph}}}{\partial t}(X_{\mathrm{ph}}) = \int_{R^3}\int_\gamma \psi^* \frac{\partial f^i}{\partial t}(X_s)\frac{K_{\mathrm{f}}\exp\left(-K_{\mathrm{f}}\|X_{\mathrm{ph}} - X_s\|\right)}{4\pi\|X_{\mathrm{ph}} - X_s\|^2(\gamma_2-\gamma_1)}\,\mathrm{d}X_s\,\mathrm{d}\gamma$$

where $\frac{\partial f^i}{\partial t}(X_s)$ is the impact ionisation rate at the point X_s. The comparison of the method with an analytical expression of the photoionisation rate is given in Section 3.2.

2.7. Poisson's equation

To reduce the Poisson's equation to a linear system, we use a first order finite element discretisation to solve for the electric potential:

$$\Phi(r,\_) = \sum_{i,j}\phi_{i,j}\chi_{i,j}(r,\_) + \__j E\chi_{i,j}(r,\_), \tag{15}$$

where $\chi_{i,j}$ is a piecewise linear function of each variable, taking the values 1 at $(r, z) = (r_i, z_j)$ and 0 at all other nodes. $\chi_{i,j}$ is given by:

$$\chi_{i,j}(r,\_) = \begin{cases} \left(1 - \frac{|r-r_i|}{\Delta r}\right)\left(1 - \frac{|\_-\__j|}{\Delta\_}\right) & \begin{cases}\text{if} & r_i - \Delta r \leqslant r \leqslant r_i + \Delta r \\ \text{and} & \__j - \Delta\_ \leqslant \_ \leqslant \__j + \Delta\_\end{cases} \\ 0 & \text{otherwise}\end{cases}$$

The function $\chi_{i,j}$ is shown in Fig. 1.

$\vec{E}$ is a constant, homogeneous background electric field of magnitude E, directed along the negative z-axis (downward as in the mesosphere).

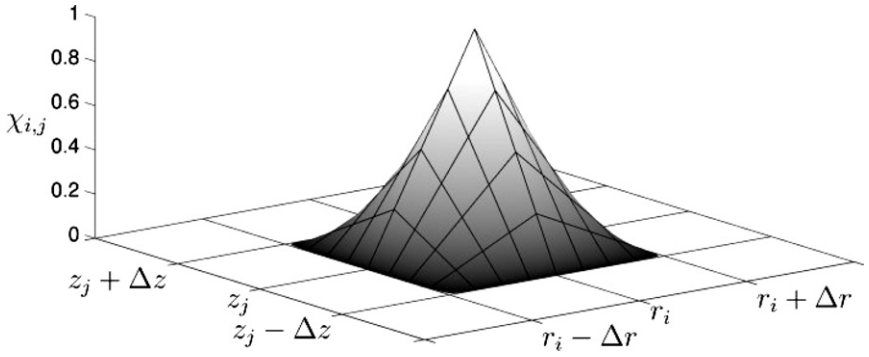

Fig. 1. The function $\chi_{i,j}$.

Using a variational formulation of Poisson equation (Eq. (2)), the coefficients $\phi_{i,j}$ are the solutions to the linear system:

$$\forall i', j', \sum_{i,j} \phi_{i,j} \int_\Omega r \nabla_{r,} \chi_{i,j}(r,) \nabla_{r,} \chi_{i',j'}(r,) \, \mathrm{d}r \mathrm{d}_{} = \int_\Omega r \rho(r,) \chi_{i',j'}(r,) \, \mathrm{d}r \mathrm{d}_{} = R_{i',j'} \tag{16}$$

The first integral is a matrix with constant coefficients determined by the grid and needs to be calculated only once. The coefficients $R_{i',j'}$ are found from the particles (see below). The linear system is solved using a LAPACK subroutine [29] based on the Choleski decomposition of the positive definite array.

When the potential on the grid is known, it is smoothed using a linear filter and then the electric field components are given by:

$$\begin{aligned} E^r_{i,j} &= \frac{\phi_{i-1,j} - \phi_{i+1,j}}{2\Delta r} \\ E_{i,j} &= \frac{\phi_{i,j-1} - \phi_{i,j+1}}{2\Delta} - E \end{aligned} \tag{17}$$

2.8. The space charge density

To solve Poisson's equation we need to find the second term of the linear system in Eq. (16):

$$R_{i',j'} = \frac{e}{\epsilon_0} \int_{r,} r \rho(r,) \chi_{i',j'}(r,) \, \mathrm{d}r \mathrm{d}_{} \tag{18}$$

It follows from Eqs. (3) and (4) that the space charge density ρ has the form:

$$\rho(r,) = \int_{r,\ \theta,\ } \sum_p \frac{p}{2\pi r} \delta(r - r_p) \delta(_ - _p) \delta(_r - _{rp}) \delta(_\theta - _{\theta p}) \delta(_ - _p) \, \mathrm{d}_r \, \mathrm{d}_\theta \, \mathrm{d}_ \tag{19}$$

where we have assumed a negative weight w_p for electrons and a positive one for ions. We obtain finally:

$$R_{i',j'} = \frac{e}{\epsilon_0} \sum_p \frac{p}{2\pi} \chi_{i',j'}(r_p, _p) \tag{20}$$

When solving for the electric field the finite element formulation of Poisson's equation avoids the calculation of densities on grid nodes. The value of the electron densities at grid nodes are needed only for plotting purposes where we use the corrected interpolation formulas given in [30] for the cylindrical particle weighting scheme.

2.9. The particle mover

In order to move the particles one needs the electric field at the particle position r_p, z_p. This is done using a first order interpolation of the electric field values from the nearest nodes (i, j), $(i, j+1)$, $(i+1, j)$ and $(i+1, j+1)$:

$$
\begin{aligned}
E^r(r_p, \_p) &= E^r_{i,j}\chi_{i,j}(r_p, \_p) + E^r_{i,j+1}\chi_{i,j+1}(r_p, \_p) \\
&\quad + E^r_{i+1,j}\chi_{i+1,j}(r_p, \_p) + E^r_{i+1,j+1}\chi_{i+1,j+1}(r_p, \_p) \\
E^{\_}(r_p, \_p) &= E^{\_}_{i,j}\chi_{i,j}(r_p, \_p) + E^{\_}_{i,j+1}\chi_{i,j+1}(r_p, \_p) \\
&\quad + E^{\_}_{i+1,j}\chi_{i+1,j}(r_p, \_p) + E^{\_}_{i+1,j+1}\chi_{i+1,j+1}(r_p, \_p)
\end{aligned}
\tag{21}
$$

2.10. The resampling algorithm

The simulation of an electron avalanche and streamer formation implies an exponential increase of the number of particles. In the simulations the number of computer particles are limited by resampling the particle population. In [31,32] a global method is described where particles are removed randomly from the simulation domain when the total particle number exceeds a limit. In this scheme, each particle has the same probability of being removed. Here we chose instead a local method because of the nature of streamers with intense ionisation regions in the streamer head. The strategy is to preferentially remove particles from cells that contain a high number of particles.

The maximum number of particles in the simulation domain $N_{\mathrm{G}}^{\max}$ is determined by the capacity of the computer. We can then define a maximum number of particles per cell i as:

$$
N_{\mathrm{L}}^{\max} = N_{\mathrm{G}}^{\max}/N_{\mathrm{G}}^{\mathrm{sum}} \log\left((10^5 - 10)\frac{\rho_i}{\rho_{\max}} + 10\right)
$$

where

$$
N_{\mathrm{G}}^{\mathrm{sum}} = \sum_i \log\left((10^5 - 10)\frac{\rho_i}{\rho_{\max}} + 10\right)
$$

and ρ_i the mean value of the electronic density at the corner nodes of the cell i. If the number of computer particles exceeds $N_{\mathrm{L}}^{\max}$ in a cell, the particle number is reduced to $3N_{\mathrm{L}}^{\max}/4$ by merging pairs of particle.

Particles are merged by first choosing randomly a particle p_1 in the cell and then locating the particle p_2 that is closest in velocity space. The two are merged creating a new particle p_3 of weight $\_{p_3} = \_{p_1} + \_{p_2}$, with position and velocity defined by the barycentric coordinates $(\_{p_1}, \_{p_2})$.

2.11. Initial- and boundary conditions

The simulations start with a plasma of equal numbers of electrons and ions at rest. The distribution functions for the particles at $t = 0$ are then:

$$
f_{\mathrm{e}}(0, r, \_, \_r, \_\theta, \_) = f_i(0, r, \_, \_r, \_\theta, \_) = n^0(r, \_)\delta(\_r)\delta(\_\theta)\delta(\_), \tag{22}
$$

The particles are placed in a subregion of the simulation domain defined by $[L^p_{rm} L^p_{rM}] \times [L^p_{\_m}, L^p_{\_M}]$ at positions:

$$
\begin{aligned}
r_p &= (i_p - \frac{1}{2})\Delta^p_r + L^p_{rm} \\
\_p &= (j_p - \frac{1}{2})\Delta^p_{\_} + L^p_{\_m}
\end{aligned}
\tag{23}
$$

with $i_p = 1 \ldots N^p_r$, $j_p = 1 \ldots N^p_{\_}$, $\Delta^p_r = (L^p_{rM} - L^p_{rm})/N^p_r$ and $\Delta^p_{\_} = (L^p_{\_M} - L^p_{\_m})/N^p_{\_}$.

The weight of a computer particle w_p is the number of real particles it represents. It can be found from the initial conditions:

$$
\_p = 2\pi r_p \Delta^p_r \Delta^p_{\_} n^0(r_p, \_p) \tag{24}
$$

The density n^0 at $t = 0$ is either constant (swarm parameter calculations) or a Gaussian (streamer simulations) in the sub-domain. Ions and electrons are placed on top of each other in pairs such that the initial space charge field is zero everywhere. Ion velocities and positions are not updated as ions are considered heavy and not responding on the time scales considered by the code. Electrons that reach the boundaries are written off (absorbing conditions).

The initial condition for the electric field is the background electric field E (directed downward as in the mesosphere). The initial value of the coefficients $\phi_{i,j}$ in Eq. (15) are therefore zero. During a simulation, the potential is held constant at the top and bottom of the cylinder ($z = 0, L_z$), keeping the background electric field constant (Dirichlet condition) and the radial electric field is held null at $r = L_r$ (Neumann condition).

2.12. The main computational scheme

In the code, electrons are first advanced during a time Δt and then the electric field is updated from the new ion and electron distributions. Then the cycle is repeated. The choice of time step Δt between two calculations of the electric field is determined by a Courant–Friedrichs–Lewy (CFL) condition associated with the mean electron velocity and the grid size. Δt is chosen to be $0.001\Delta_{\backslash}/\overline{\backslash}$, where $\overline{\backslash}$ is the mean electron velocity in the background electric field E. This ensures that changes to the charge density distribution between electric field updates are small and thus the stability of the simulation.

The time step for particle updates, $\Delta^c t$ introduced earlier in Section 2.3, must be below $\Delta^c_{\max} t$. If the electric field times step Δt is below this limit fields and particles can be updated using the same time steps. If Δt is larger than the limit of the particle updates, particles are updated N_{sub} times with a time step $\Delta^c t < \Delta^c_{\max} t$ before updating the field. In this case the parameters are chosen such that $\Delta t = N_{\text{sub}} \Delta^c t$.

The code has been parallelised to take advantage of multiprocessor computers. The largest computational load comes from updating the particles. The code is then parallelised by distributing particles between the processors, so each processor updates a subset of particles. To do this, each processor must also have access to the electric potential distribution which is passed to all processors after each electric field update. The main scheme of the PIC-MCC code is presented in Fig. 2.

A typical run consists of:

Initial conditions.

- The initial electric field on the grid is loaded onto each computer.
- The initial computer particles are loaded and shared between the processors.

The main update cycle for the electric field (Δt).

- The cycle for the particles updated N_{sub} times.
  - Each processor moves its particles the time step $\Delta^c t$.
  - Each processor performs collisions during $\Delta^c t$ according the Monte Carlo scheme.

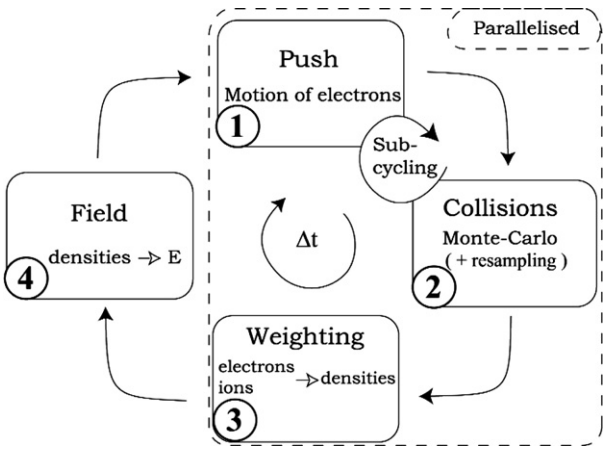

Fig. 2. The PIC-MCC scheme.

– Each processor recalculates the electron and ion densities according the new positions of the particles.
– One processor gathers and sums the densities from all processors and calculates the electric field from Poisson's equation.
– The processor distributes the updated field to all processors.

3. Code validation

All tests presented in this section are performed using the cross sections of the BOLSIG package [23] with their assumption of isotropic scattering. The basic parameters, including the swarm parameters, related to the drift of electrons through a gas in a constant, uniform electric field are first determined. The results are compared to the results of the BOLSIG code [23], which is based on the two-term Legendre expansion solution of the Boltzmann equation [33]. Independent validation of the particle weighting scheme and of the Poisson solver has also been done, but is not presented here. Then test runs of the photoionisation model is compared with an analytical formula commonly used in fluid simulations [34,16,50,35]. Finally, a full simulation of streamer formation in the mesosphere, is compared with recent fluid simulation [16].

3.1. Test without space charge fields

We first test the electron energy distribution in the presence of a constant background electric field. A cloud of electrons is loaded into the simulation domain. The background electric field is specified to be $E/P = 300$ Td, where P is the pressure of the neutral gas. The electric field is not updated from the space charge fields, but remains constant. When steady state has been reached, the distribution function is reconstructed from the particles and compared to the results of the BOLSIG code. The test is performed using the same model for ionisation as in BOLSIG, i.e. the remaining energy after the collision $\epsilon_{in} - \epsilon_{co}$, is shared equally between the energy of the scattered electron ϵ_{sc} and the energy of the secondary electron ϵ_{ex}. The result is shown in Fig. 3. There is a good agreement between the codes except at the peak near 2 eV. The observed discrepancy could be caused by the BOLSIG code being limited to a two-term Legendre approximation, however, a proper analysis of the discrepancy is beyond the scope of this article. Instead, the reader is referred to Pitchford et al. [33] for comparisons between two-term and up to six-term approximations. Next, key swarm parameters from the PIC-MCC and the BOLSIG codes are compared. The parameters are the mobility, μ (the ratio between the drift velocity and the field), the Townsend coefficient, α (the ratio between the ionisation frequency and the drift velocity), the attachment coefficient, a (the ratio between the attachment frequency

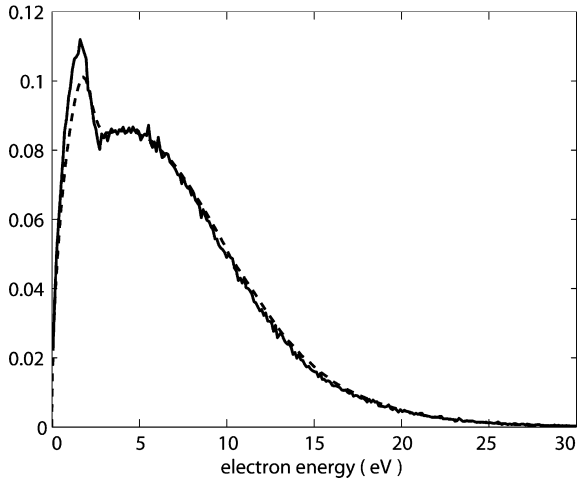

Fig. 3. The normalised electron distribution function of electrons drifting in a reduced electric field of 300 Td. The BOLSIG code (dotted line) and the PIC-MCC model (full line).

and the drift velocity) and the mean electron energy, $\bar{\epsilon}$. The parameters are determined by following a cloud of electrons drifting through a neutral gas for a range background electric field values.

The electron drift energy is found from the electron distribution function in energy $n_e(r, z, \epsilon)$:

$$\bar{\epsilon}(r,\,) = \int_{\epsilon} \epsilon n_e(r,\,,\epsilon)\,\mathrm{d}\epsilon$$

The drift velocity $\bar{}_{\,}$ along the electric field $E = E_z$ is found from the electron distribution function:

$$\overline{}_{\,} = \int_{r,\,\theta,\,} {}_{\,} f_e(t, r,\,,\ r,\ \theta,\ \,)\,\mathrm{d}\ r\,\mathrm{d}\ \theta\,\mathrm{d}\ \,$$

The mobility is then defined as:

$$\mu = \frac{\overline{}}{E_{\,}}$$

The Townsend coefficient is:

$$\alpha(r,\,) = \frac{\bar{\gamma}_i(r,\,)}{\overline{}(r,\,)}$$

where $\gamma_i(\bar{r},\,)$ is the ionisation frequency:

$$\bar{\gamma}_i(r,\,) = \int_{\epsilon} n_n \sqrt{\frac{2e\epsilon}{m_e}}\sigma_i(\epsilon) n_e(r,\,,\epsilon)\,\mathrm{d}\epsilon$$

The attachment coefficient is defined in a similar way:

$$a(r,\,) = \frac{\bar{\gamma}_a(r,\,)}{\overline{}(r,\,)}$$

where $\overline{\gamma_a}$ is the attachment frequency. The parameters obtained for the two codes are shown in Fig. 4. The two methods are generally in very good agreement. There are some discrepancies for high electric fields which again could be caused by the two-term Legendre approximation of the BOLSIG code.

3.2. Test of the photoionisation model

The photoionisation model adopted in the particle code is compared with the analytical expression given in [35] that gives the photoionisation rate $S_{ph}(r, z)$ at the point (r, z) as a function of the photon production rate $I(r_s,\,{}_s) = \psi^* \frac{\partial f^i}{\partial t}(r_s,\,{}_s)$ at the point (r_s, z_s). In cylindrical coordinates, it is:

$$S_{\mathrm{ph}}(r,\,) = \int_{\mathrm{d}r_s} \int_{\mathrm{d}\,{}_s} I(r_s,\,{}_s) M_{\mathrm{ph}}(r, r_s, \|\,-\,{}_s\|)\mathrm{d}\,{}_s\,\mathrm{d}r_s \tag{25}$$

with

$$M_{\mathrm{ph}}(r, r_s, \|\,-\,{}_s\|) = \int_{\gamma_1}^{\gamma_2} \int_0^{2\pi} \frac{r_s K_{\mathrm{f}} \exp(-K_{\mathrm{f}} R(\phi_s))}{4\pi R^2(\phi_s)(\gamma_2 - \gamma_1)}\,\mathrm{d}\phi_s\,\mathrm{d}\gamma$$

and $R(\phi_s) = \sqrt{r_s^2 + r^2 + (\,-\,{}_s)^2 - 2rr_s\cos\phi_s}$

In the particle code the photoionisation model is tested by considering the effect of a single computer electron. Assuming the photon production rate at the location (r_s, z_s) is given by $I(r_s, z_s) = \delta(r_s - r_S)\delta(z_s - z_S)/\Delta t$, from Eq. (25) the resulting photoionisation density after the arbitrary time step Δt is:

$$\Delta t S_{\mathrm{ph}}(r,\,) = \int_{r_s} \int_{\,{}_s} \Delta t I(r_s,\,{}_s) M_{\mathrm{ph}}(r, r_s, \|\,-\,{}_s\|) = M_{\mathrm{ph}}(r, r_S, \|\,-\,{}_s\|)$$

To calculate this photoionisation density in our particle code we place a single computer electron at the position (r_S, z_S) with a weight $w_p = 2\pi r_S$, and force this particle to undergo one ionizing collision during the time

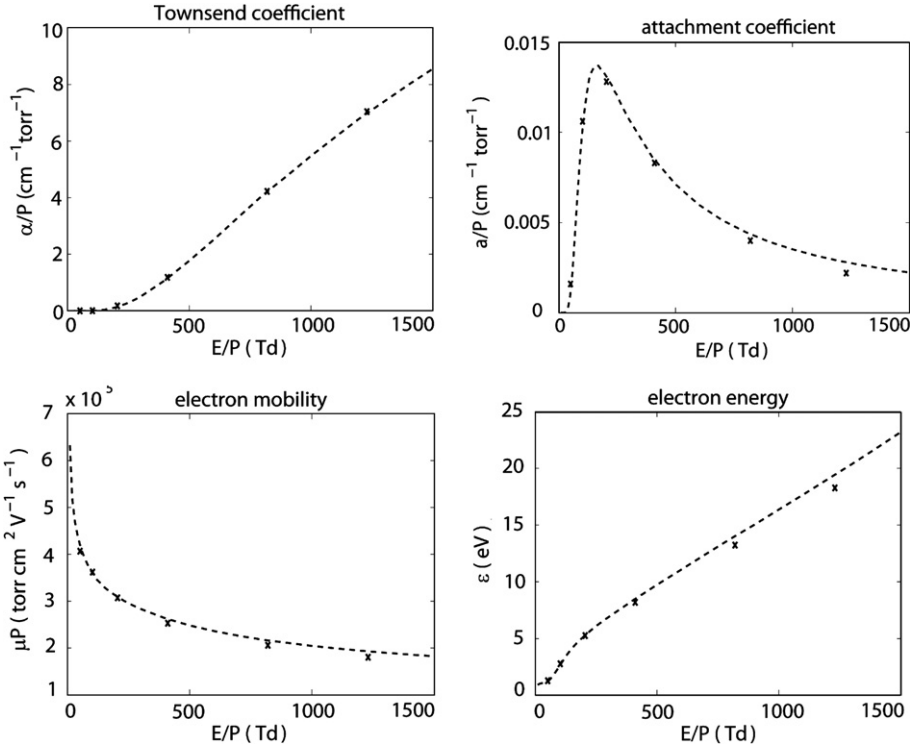

Fig. 4. The swarm parameters for air (80% N_2 and 20% O_2) as functions of electric field calculated from the BOLSIG code (dotted line) and the PIC-MCC code (markers).

step Δt. We further force the relative emissivity ψ^* to one and we fix the number of emitted photons to two values: 10^4 and 5×10^6 to test the impact of limitations in the statistics of the photon representation. Finally we calculate the photoionisation density after a time Δt. The results for the two values of the emitted photons are presented in Figs. 5 and 6. The point source is located at $r_S = 15$ m, $z_S = 100$ m in air of density 1.61×10^{15} cm^{-3}, corresponding to 70 km altitude.

As seen from the figures the general agreement between the methods is good. However, some differences are introduced at long distances from the point source when the number of emitted computer photons is not able to represent the analytical formulation. In the particle code a computer photons represents a real photon except at high emissivities (high electron weight) where a limit of 10^4 computer photons is imposed and these then represent many real photons. The large number of electrons being a source of photons in a streamer simulation tends to reduce the statistical noise.w

3.3. Comparison with fluid simulation

The results of streamer formation in the PIC-MCC code are now compared to the fluid simulations of Liu and Pasko [16] of streamer propagation in the mesosphere at 70 km altitude where sprites are generated. Following Liu and Pasko [16], a streamer is initiated from a plasma cloud with peak density 5×10^{11} m^{-3} and Gaussian spatial distribution with scale 3 m. The particles are loaded uniformly into a sub-region as described earlier, with the weight of the particles following the Gaussian distribution. The air density is 1.61×10^{15} cm^{-3}, corresponding to 70 km altitude and the air is assumed to be composed of 80% nitrogen and 20% oxygen. At this altitude the threshold for breakdown, where the Townsend coefficient equals the attachment coefficient, is $E_k = 220$ V m^{-1}. Following [16], the background electric field is set to $E = 1.5E_k = 330$ V m^{-1}. In this background field $\mu = 600$ m^2 V^{-1} s^{-1} and $\alpha - a = 0.73$ m^{-1}. These are given locally and are updated at each time step of the electric field. The test run is performed using the same

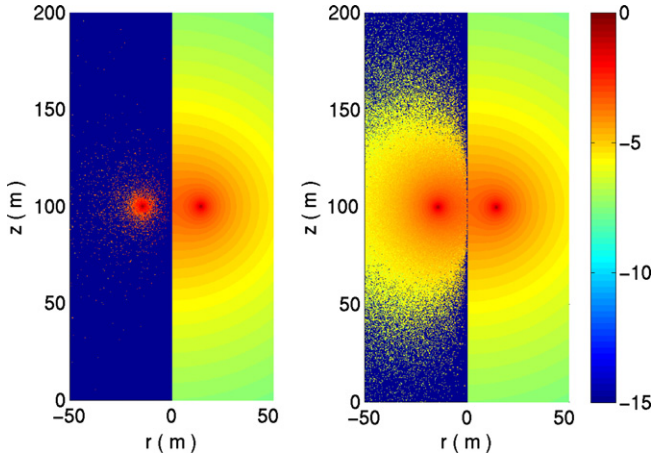

Fig. 5. Comparison of photoelectron density from a point source located at $r_S = 15$ m, $z_S = 100$ m emitting a fixed number of computer photons of 10^4 (left panel) and 5×10^6 (right panel). On each panel the result from the particle method is given for $r < 0$ whereas the analytic expression of M_{ph} is plotted for the $r > 0$. The background color of the particle model corresponds to zero density.

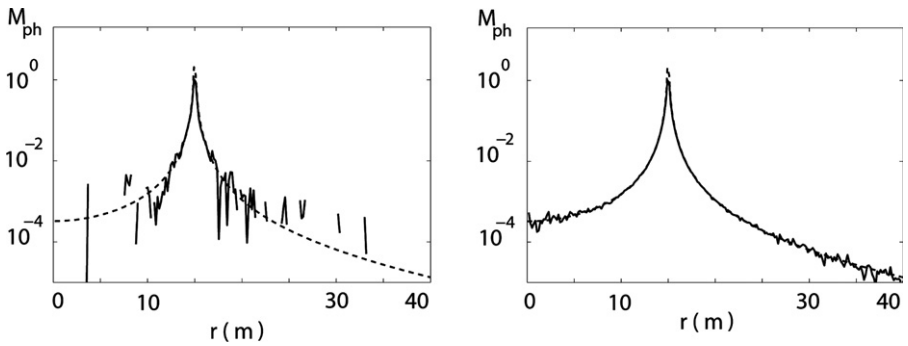

Fig. 6. Comparison of photoelectron density from a point source located at $r_S = 15$ m, $z_S = 100$ m emitting a fixed number of computer photons of 10^4 (left panel) and 5×10^6 (right panel). The result from the particle method is plotted as full line and the analytical expression M_{ph} as dashed line.

simulation parameters and the same cross sections as shown in the previous subsections for testing of the swarm parameters but the ionisation model comes from Opal et al. referenced in Section 2.4.

The results are presented in Fig. 7. The electron density is shown on the top panels and the magnitude of the electric field (the background and the space charge fields) on the bottom panels at three different times. The background electric field is directed downward. A bipolar streamer is developing with the positive streamer propagating in the downward direction and the negative streamer in the upward direction. The simulation reproduces the main characteristics of streamer propagation and is in qualitative agreement with the results of fluid simulation [16].

A quantitative comparison of the fluid and PIC-MCC simulations is shown in Fig. 8. The electron density and electric fields on the axis of symmetry are shown at three different times. The top panel is the fluid code electron density, the second panel is the PIC-MCC electron density, the third panel is the fluid electric field magnitude, and the bottom panel is the PIC-MCC electric field. While there is good agreement between the two simulations, there are also some differences: The propagation speed of the ionisation front of the positive streamer (propagating toward lower z-values) is smaller in the particle simulation than in the fluid simulation, with the distance reached at 40 μs being lower by about 7.5%. The negative streamer velocity (propagating toward higher z-values), on the other hand, is higher by about 7%. Comparing the electric fields

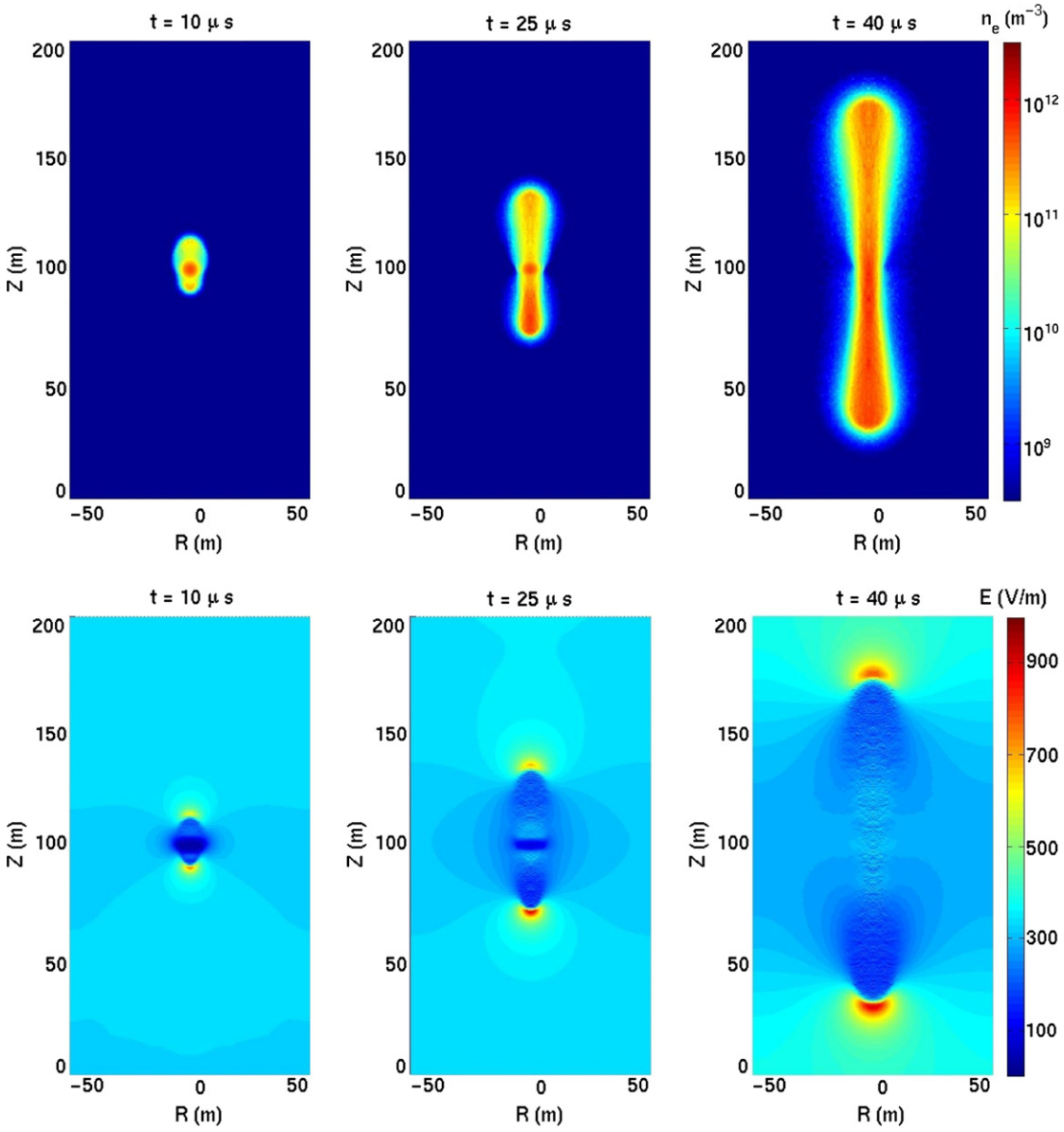

Fig. 7. Electron density (top) and electric field magnitude (bottom) at $t = 10$ μs, 25 μs and 40 μs for $E = 1.5E_k$.

the peak values in the positive streamer tip is lower in the particle simulation by about 10% whereas the values agree well in the negative streamer tip. There are potentially several sources of these discrepancies including differences in the swarm parameters, the photoionisation model, numerical artificial diffusion or from the local field approximation used in the fluid model. However, given that the two codes are based on different numerical approaches, the results are considered in excellent agreement. The interested reader is referred to [36] for a comparison of simulations in a 1D PIC model and a 1D fluid model and [16,34] for a discussion of the representation of photoionisation. Finally, the influence of numerical errors in fluid simulations is described in [37]. We add that the PIC-MCC model, while allowing studies of particle acceleration and their effect on streamer dynamics, is noisy because of limitations on the number of particles that can be simulated. The rather good comparison with fluid simulations shown here ensures that the influence of noise on the streamer formation and propagation is small.

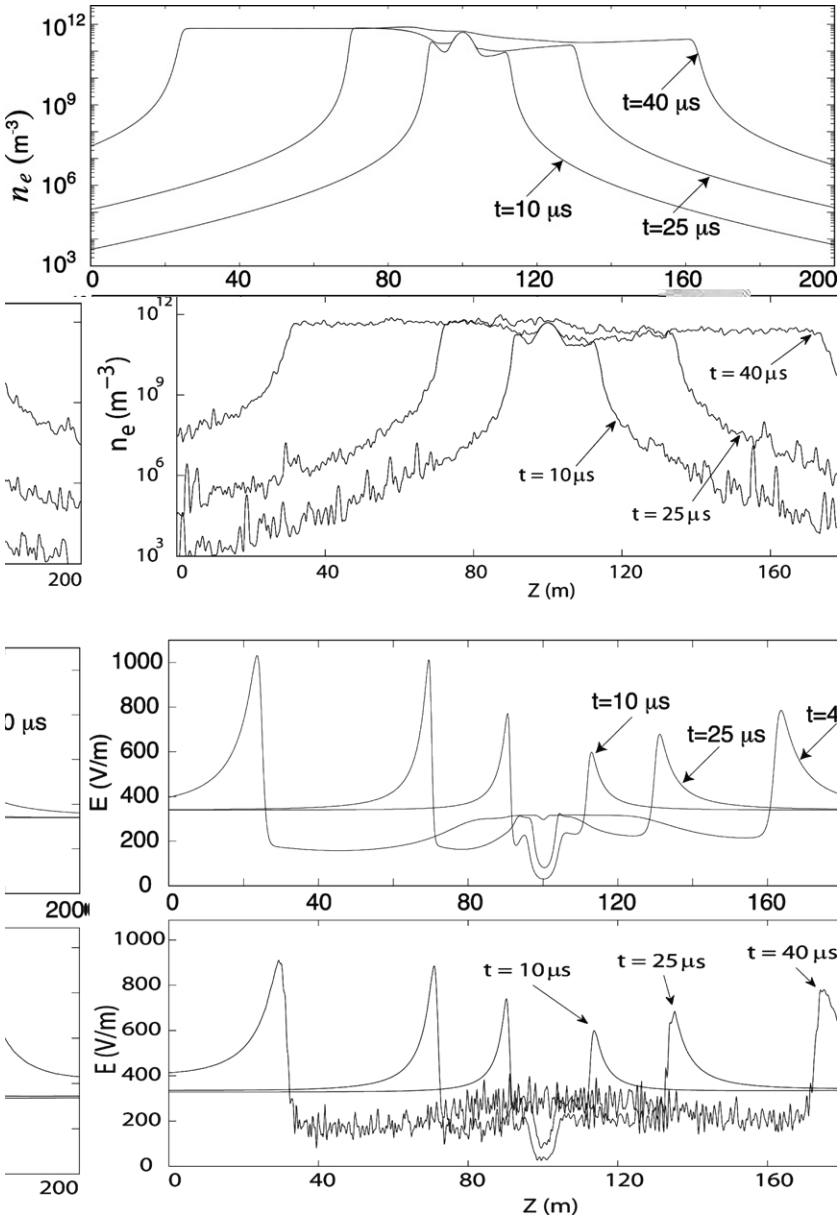

Fig. 8. Simulations of streamer development in the mesosphere by a fluid code [16] and the particle code for $E = 1.5E_k$. (a) The on-axis electron density in the fluid simulation and (a′) in PIC-MCC. (b) The on-axis electric field (directed toward the left) in the fluid simulation and (b′) in PIC-MCC. Data are shown for $t = 10$ μs, 25 μs and 40 μs. The simulations are for the same initial plasma-, electric field- and neutral atmosphere parameters.

4. Energetic electrons and photoionisation in streamers

It has been suggested that the relativistic runaway electron electric discharge, operates in sprites [38]. This mechanism assumes a population of energetic (relativistic) seed electrons at energies above $\simeq$100 keV created by cosmic ray ionization of the atmosphere, which form an avalanche carried by energetic electrons. At these energies the collisional cross sections of air decrease with energy until relativistic effects take over at energies above a few MeV. The higher the electron energy in this energy range, the lower the frictional force exerted by the air constituents on the electrons. This relativistic runaway electron discharge has a threshold electric field

that is $\simeq$10 times smaller than the conventional threshold field and should therefore be triggered before the conventional discharge, provided the needed high energy seed electrons are present.

The frictional force F_D can be defined by:

$$F_D(\epsilon) = -\sum_k n_n \sigma_k(\epsilon)\delta\epsilon_k \tag{26}$$

where $\delta\epsilon_k$ is the energy loss in a k collision.

The acceleration of an electron by the combined action of the frictional force and the force exerted by the electric field $\mathbf{F}_E = -e\mathbf{E}$ is given by:

$$d\epsilon/dt = \mathbf{v}\cdot\mathbf{F_E} + \mathbf{v}\cdot\mathbf{F_D} = \ (-eE\cos\beta - F_D) \tag{27}$$

where β is the angle between the electric field and the velocity of the particle and e is the elementary charge (positive). The smallest electric field required for acceleration of the electron is found when $\cos\beta = -1$ which is where the two forces are aligned but pointing in opposite directions. Here an electron gains energy when $F_E > F_D$ and loses energy when $F_E < F_D$.

Fig. 9 shows the frictional force corresponding to the cross sections of the PIC-MCC model and the force from an electric field $E = 3E_k$ acting on an electron. The forces cancel for two energies, $\epsilon_1 \simeq 31.5$ eV and $\epsilon_2 \simeq 1215$ eV. For electrons with $\cos\beta = -1$, the lower energy represents a stable equilibrium, where an electron with an energy $\epsilon < \epsilon_1$ is accelerated and $\epsilon_2 > \epsilon > \epsilon_1$ is decelerated. A conventional discharge driven by thermal electrons will have electrons with energies that'oscillates' around the stable equilibrium ϵ_1. The higher energy represents an unstable equilibrium, where an electron with $\epsilon > \epsilon_2$ continue to be accelerated. This is the runaway process. However, the threshold energy ϵ_2 is only a necessary condition for the runaway regime since it assumes $\cos\beta = -1$. A sufficient condition must consider angular scattering of electrons. Depending on the scattering model, although an electron can satisfy the criterion at a given time, scattering will act to reduce the action of the electric field such that an electron may loose energy and diffuse out of the runaway regime again. The choice of the scattering model is therefore important in the runaway process (see for instance [11]).

The threshold electric field for the relativistic runaway breakdown is seeded and carried by electrons with energies well above ϵ_2. Theories predict about 10 times lower electric field threshold than for conventional breakdown because the frictional force is small at these energies. As the quasi-electrostatic field in the mesosphere from a cloud-to-ground lightning discharge is thought to require extremely large lightning discharges for triggering conventional breakdown, the relativistic runaway mechanism has been suggested to explain why

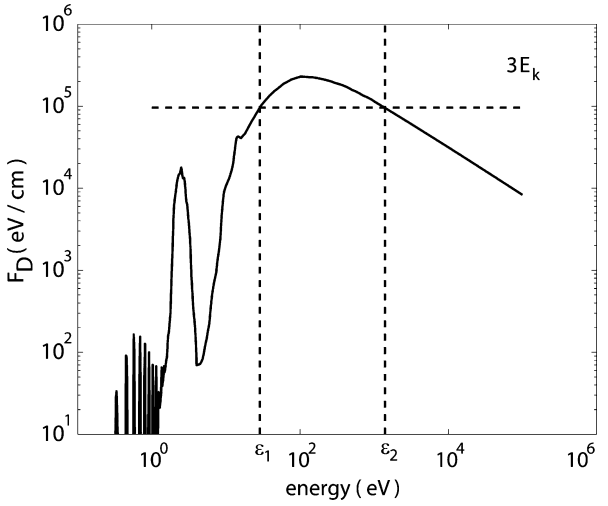

Fig. 9. The frictional force in air composed of 80% nitrogen and 20% oxygen at atmospheric pressure. Also shown is the electric force acting on an electron for $E = 3E_k$. The two forces are of equal magnitude at the energies ϵ_1 and ϵ_2.

sprites in the mesosphere occur quite frequently anyway [39]. In addition, electric field values measured in the stratosphere and mesosphere from balloons have not been observed to reach the conventional breakdown field, but fit rather well with the maximum field strength predicted by the relativistic breakdown field [40]. Finally, a runaway electron electric discharge will produce a beam of relativistic electrons directed upward and out of the atmosphere, which will produce Bremsstrahlung radiation. It has been suggested that the Terrestrial gamma-ray Flashes (TGFs) [38] observed from the Compton γ-Ray Observatory (CGRO) satellite [41] and the (RHESSI) satellite [12] are the result of this process.

The process of relativistic runaway electron breakdown has received considerable attention since the discovery of TGFs. Observations of γ-rays now come from laboratory sparks [42,15], from lightning [13,43], and in rocket-triggered lightning [44–46] and are interpreted as Bremsstrahlung from relativistic electrons accelerated in the discharge. Earlier observations from balloons in thunderstorms have shown a build-up of X-ray emissions in the period preceding a lightning discharge after which the radiation disappears, suggesting the production of energetic electrons with increasing electric field [14].

In [11], it is suggested that energetic electrons are produced also in conventional discharges primarily carried by electrons with energies below ϵ_2. They studied the generation of runaway electrons from thermal streamers using a 1D Monte Carlo model and an empirical 1D model of the electric field and the electron density through a streamer. Several models of electron scattering are compared and they obtain a significant production of runaway electrons if the electric field in the negative streamer tip is of sufficient magnitude and the scattering model for increasing electron energy tends rapidly toward the forward direction. For instance, a streamer propagating in a background field of $3E_k$ is shown to produce energetic electrons in its negative tip where the field is assumed to reach $10E_k$. A probable scenario is then introduced suggesting that the streamer region of lightning leaders could contribute to the production of X- and γ-rays.

4.1. The electron distribution function in high electric fields

In the following we discuss further the question of acceleration of electrons in conventional streamers. First we determine the distribution function of electrons in electric fields from $3E_k$ to $10E_k$. To obtain the distribution function, we proceed as in Section 3.1, but with the anisotropic scattering model introduced Section 2.5 and the ionisation model from Opal et al. [22], introduced in Section 2.4. The results are presented in Fig. 10 for electrons drifting in air under 1 atm pressure in a field of $3E_k$, $5.5E_k$, $7.5E_k$ and $10E_k$. The two lowest fields correspond to ϵ_2 equal to 1215 eV and 371.2 eV. For the two highest fields, the force from the electric field is always above the frictional force as defined for $\cos\beta = -1$ and thus some electrons can in principle be accelerated to the runaway regime.

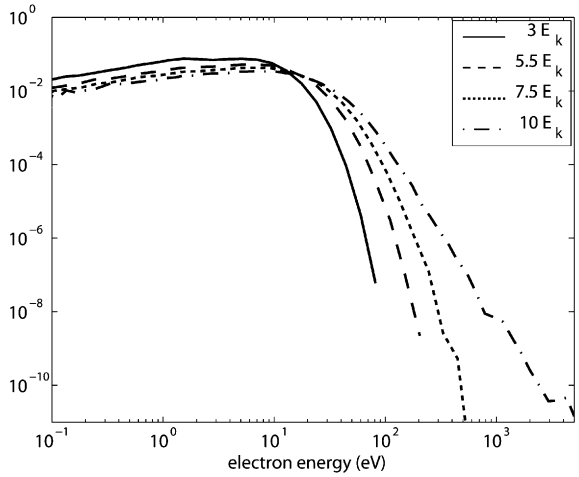

Fig. 10. The distribution function of electrons drifting in a field of $3E_k$, $5.5E_k$, $7.5E_k$ and $10E_k$ in air at 1 atm pressure composed of 80% nitrogen and 20% oxygen at atmospheric pressure.

For $E = 3E_k$ and $5.5E_k$, the maximum electron energy observed in the simulation are ~80 eV and ~175 eV which are below the minimum runaway threshold ϵ_2. For $E = 7.5E_k$, a few runaway electrons are observed compared to about 12 million computer particles of the simulation. For $E = 10E_k$ many electrons are in the runaway regime.

In the case of the two high electric field simulations, electrons are found with energies that are above even the threshold field corresponding to $E = 3E_k$ where $\epsilon_2 \simeq 1215$ eV. These results suggest that electrons can be accelerated in the high field region of a streamer tip into the runaway regime of the lower field region in front of the streamer. The first condition is that the streamer tip field is above the value corresponding to $F_E = F_D$ or to $E \simeq 7.5E_k$ for the atmosphere at 1 atm pressure. The second condition is that electrons travel enough time in the enhanced field region to reach runaway energies. This is the self-acceleration of electron first introduced by [47] and described in [11].

4.2. Effects of photoionisation

All streamer properties scale with altitude except the photoionisation due to an increased quenching with decreasing altitude of those exited nitrogen states that lead to photoionisation of oxygen [7,16,48]. To discuss the effect of photoionisation on streamer development and formation of runaway electrons, we present 3 self-consistent simulations of streamer ignition in air with a background electric field of $E = 3E_k$, but with different levels of photoionisation. Two simulations are with full photoionisation at air densities 1.61×10^{15} cm^{-3} and 8.5×10^{18} cm^{-3}, corresponding to 70 km and 10 km altitude. The third simulation is without photoionisation at 70 km altitude. The electric field threshold for conventional breakdown at these altitudes is 220 V m^{-1} (70 km) and 1170 kV m^{-1} (10 km). The simulation is performed with the scattering model presented in Section 2.5 [26] on the same mesh that is used in Section 3.3.

Figs. 11 and 12 show the evolution in time of the electron density and the electric field along the center axis of the streamer during the initial stage of streamer formation. On the figures the densities and fields are scaled to the common altitude of 70 km for easier comparison. Time and distance scale as $\sim 1/n_{air}$, where n_{air} is the atmospheric air density. The electron density scales as $\sim n_{air}^2$ and the electric field scales with the electric

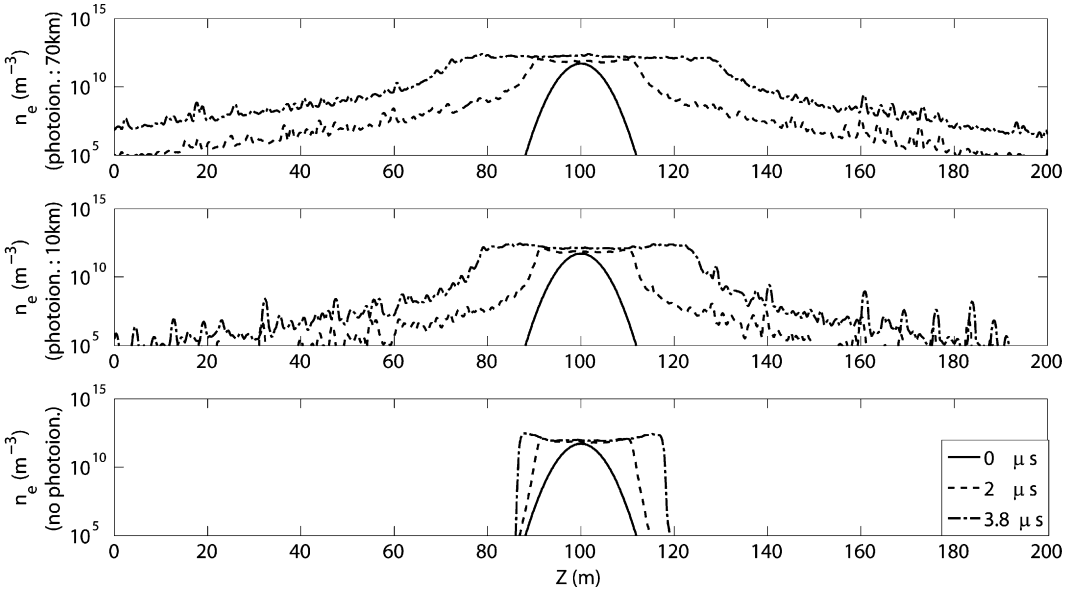

Fig. 11. The evolution of the electron density for a streamer propagating in a background electric field $E = 3E_k$ for a photoionisation level corresponding to 70 km (top), 10 km (middle) and without photoionisation (bottom). The results corresponding to 10 km are rescaled to the altitude of 70 km (see text).

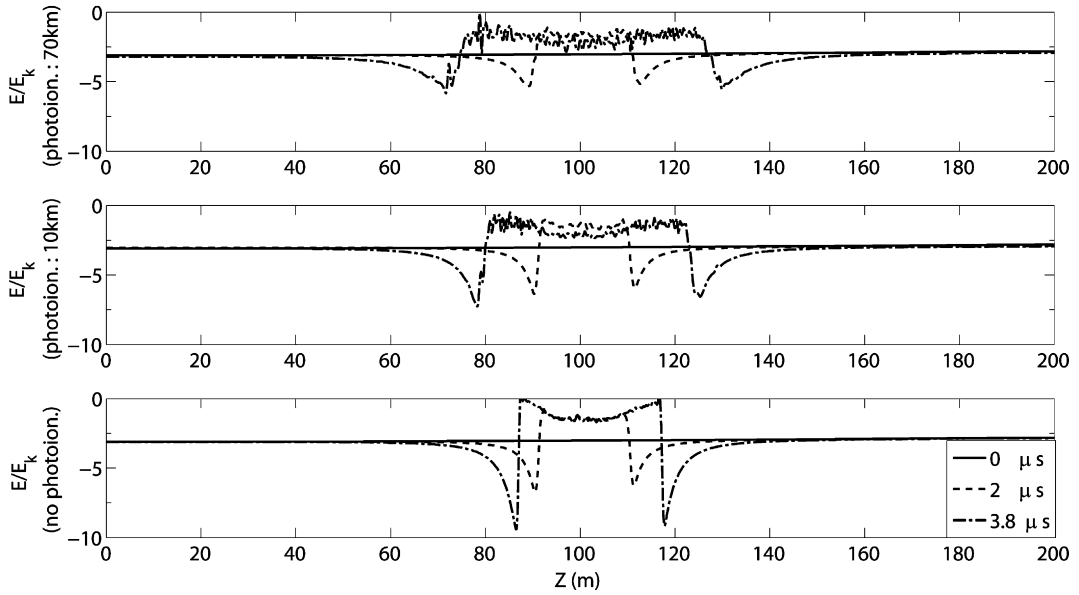

Fig. 12. The evolution of the electric field for a streamer propagating in a background electric field $E = 3E_k$ for a photoionisation level corresponding to 70 km (top), 10 km (middle) and without photoionisation (bottom). The results corresponding to 10 km are rescaled to the altitude of 70 km (see text).

threshold field E_k which scales as $\sim n_{\mathrm{air}}$. The Fig. 14 present the density at the time of 4.9 μs, for the three test cases.

From Figs. 11 and 12 it is clear that the streamer propagation speed increases with higher photoionisation level and reaches its highest (scaled and unscaled) value at high altitudes. The field enhancement, however, is smaller because the electron density gradients are progressively smaller in the streamer tip with stronger photoionisation. The consequence of this is that at higher altitudes it becomes relatively more difficult to accelerate thermal electrons in streamer tips to energies that are in the runaway regime in the atmosphere surrounding the streamer. This point is further illustrated in Fig. 13 which shows the peak values of the electric field in the negative streamer head and the maximum electron energy obtained in the three simulations. It shows that at 10 km altitude, the field in the streamer tip with photoionisation included reaches $E \simeq 7.5E_k$ which is just

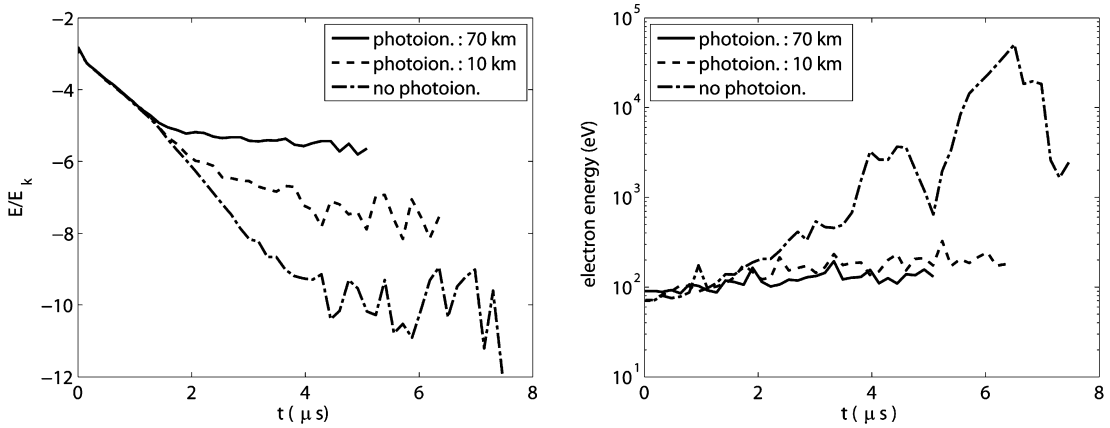

Fig. 13. The evolution of the peak electric field in the negative streamer head (left panel) and of the maximum electron energy (right panel) for a streamer propagating in a background electric field $E = 3E_k$ for a photoionisation level corresponding to 70 km, 10 km and without photoionisation. The results corresponding to 10 km are rescaled to the altitude of 70 km (see text).

marginal to create runaway electrons as shown in the previous section. At high altitudes, the field reaches $E \simeq 5.5E_k$ which is too small to create runaway electrons. For the last test case, without photoionisation, the field reaches values $E \simeq 10E_k$, and runaway electrons are generated. We note at this point that photoionisation in moist air is reduced due to quenching on water molecules [49]. This will have the effect of increasing the streamer tip field in thunderstorm clouds relative to the results of the model presented here for dry air. For more details on photoionisation effects on streamer propagation one can refer to [50,16,48,51].

Fig. 14 shows the three streamers at $t = 4.9$ μs. The effects of photoionisation is seen to create an extended region around the bipolar streamers which allows both the positive and the negative streamers to propagate faster, but tends to reduce the gradients of the electric space charge fields at the streamer tips. The streamers that include photoionisation show no sign of branching whereas the negative streamer without photoionisation shows early signs of branching. The effect of photoionisation on branching is discussed further in Refs. [50,48], here we note that the branching is stimulated by energetic electrons traveling ahead of the streamer. This will be explored further in the following subsection.

4.3. Effects of runaway electrons on streamers

To study runaway production and its effect on streamer development further a simulation was done with the photoionisation turned off. The parameters of the simulation were the same as presented in the previous subsection with $E = 3E_k$ corresponding to $\epsilon_2 \simeq 1215$ eV. The electron density of the negative streamer is shown in Fig. 15 for $t = 6.5$ μs (top left), $t = 8.1$ μs (top right), $t = 9.7$ μs (bottom left) and $t = 11.3$ μs (bottom right). The plots are cylinder symmetric reflecting the code geometry. On the right part of each frame trajectories of electrons with energies above the runaway threshold $\epsilon_2 \simeq 1215$ eV are shown as white curves for the time corresponding to the preceding 1.6 μs.

High-energy electrons escaping the negative streamer head are creating ionization trails ahead of the streamer and the trails modify the dynamics of the streamer head by inducing branching. Energetic electrons are then likely to play a role in streamer development even in the case where photoionisation is included, provided the field in the streamer tip is of sufficient magnitude to support acceleration of electrons into the runaway regime as defined for the lower field region of the atmosphere surrounding the streamer. While this simulation brings home the points of the underlying physics, it is worthwhile to note that one computer electron represent many real electrons. In a real streamer it is expected that the region in front of the streamer will be ionized by a

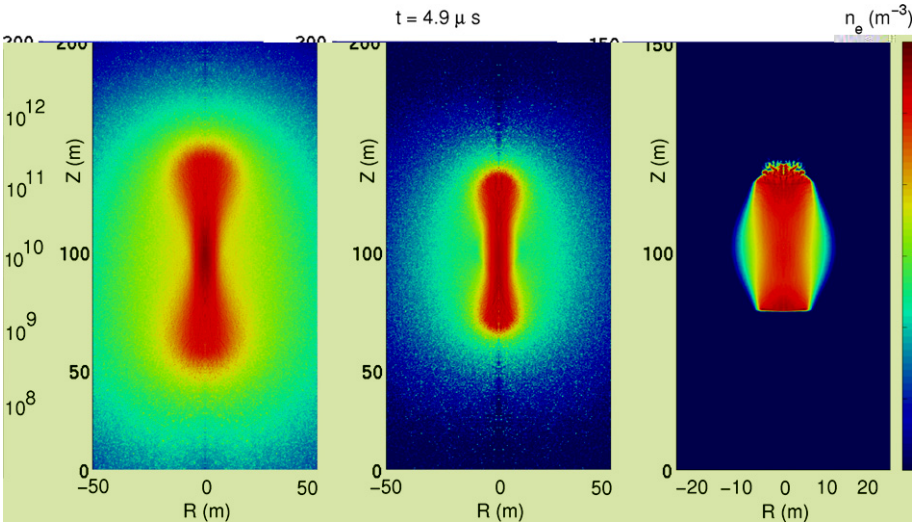

Fig. 14. The electron density at $t = 4.9$ μs for a streamer propagating in a background electric field $E = 3E_k$ for a photoionisation level corresponding to 70 km (left), 10 km (middle) and without photoionisation (right). The results corresponding to 10 km are rescaled to the altitude of 70 km (see text).

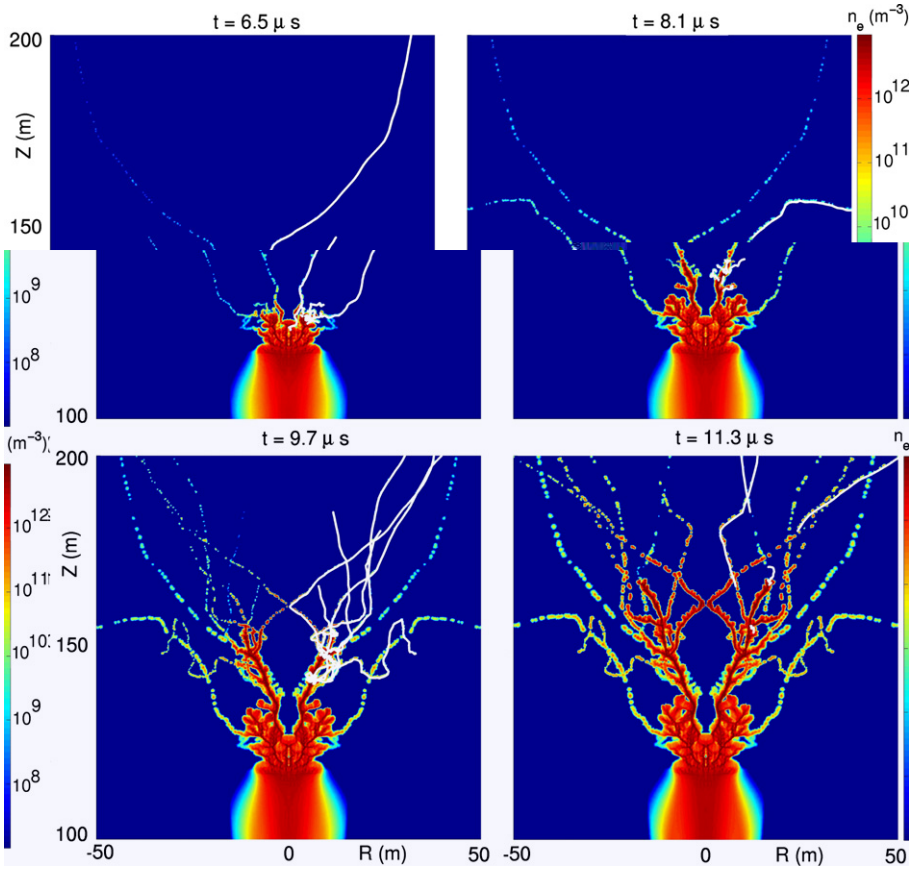

Fig. 15. The electron density at $t = 6.5$ μs (top left), $t = 8.1$ μs (top right), $t = 9.7$ μs (bottom left) and $t = 11.3$ μs (bottom right). The parameters of the simulation were the same as presented in the previous subsection with $E = 3E_k$ corresponding to $\epsilon_2 \simeq 1215$ eV. Trajectories of electrons with energies above the runaway threshold are shown as white curves for the time corresponding to the preceding 1.6 μs (see text).

multitude of electrons and that branching will be less pronounced. In some respect, runaway electrons then resemble photons in their effect on ionizing the region surrounding a streamer, except runaway electrons are more directional toward the propagation direction of the negative streamer.

5. Discussion

We have presented a 2D, axi-symmetrical particle code and applied it to the problem of streamer formation in air in the presence of a homogeneous background electric field. The code is based on a standard Particle-in-Cell plus Monte Carlo Collision method. It includes an algorithm for resampling of the electrons to maintain their number below a maximum that can be handled by the computer system running the code. The code also includes a model for ionisation by photons emitted from excited air constituents in the streamer tip. The code has been validated without space charge fields, where single particle motion dominates, by comparing its results with a Boltzmann code [23], and for large space charge fields, where collective effects dominate, by comparing streamer formation with simulations based on the drift diffusion model of a discharge [16].

The code allows the fields and the densities to develop self-consistently. In addition, as the code is in 2D cylindrical geometry, the space charge fields and their spatial variations, have realistic spatial dependencies, at least during the initial phase of streamer formation presented here, where the axi-symmetrical 2D geometry mimics a full 3D representation. This point is crucial for studies of streamers where space charge fields dominate the physics. Energisation of thermal electrons into the runaway regime has been studied for a range of

background electric field values. For air, the requirement for production of runaway electrons drifting in a constant background electric field is for the field to exceed $\simeq 7.5E_k$. This level is close to the point where the electric force on an electron exceeds the maximum value of the frictional force experienced by an electron – found at ~100 eV. It has also been shown that provided the field in the streamer tip is high enough, electrons may escape the streamer tip region with energies in the runaway regime also in the lower field region of the atmosphere surrounding the streamer, in the process creating ionization trails that modify streamer development.

Photoionisation has been shown to increase streamer propagation speeds and decrease the electric field in streamer tips. It has also been demonstrated that photoionisation plays an increasing role with increasing altitude. The effect is that it becomes progressively harder to accelerate electrons into the runaway regime with higher altitude. The conclusion is then that the process of thermal electron acceleration to the runaway regime could play a role at the lower altitudes in connection with lightning and electrification of clouds whereas it is unlikely in sprites in the mesosphere at 70 km altitude where unrealistically high background fields are needed. Refs. [52,53] reported measurements of electric field in sprite streamer tips of $3E_k$. For runaway electrons to be generated here, the discharge must be ignited by electrons already in this regime and not by thermal electrons considered in this paper.

X- and γ-rays observed in thunderclouds [14], from lightning [13,43], and in laboratory sparks in air [15], are then not necessarily a signature of a relativistic runaway discharge seeded and carried by runaway electrons [54], but may be a conventional thermal discharge producing bursts of energetic electrons. These may in turn develop into a relativistic runaway discharge provided the temporal and spatial variations of the background electric field permit this. This would be a case where a thermal discharge ignites a relativistic runaway discharge.

Acknowledgments

This research was sponsored through the CAL Research Training Network by the European Commission under the Contract HPRN-CT-2002-00216. The authors thank the referee for valuable comments.

References

[1] T. Neubert, On sprites and their exotic kin, Science 300 (5620) (2003) 747–749.
[2] D.J. Boccippio, E.R. Williams, S.J. Heckman, W.A. Lyons, I. Baker, R. Boldi, Sprites, ELF transients, and positive ground strokes, Science 269 (5227) (1995) 1088–1091.
[3] S.A. Cummer, U.S. Inan, Measurement of charge transfer in sprite-producing lightning using elf radio atmospherics, Geophys. Res. Lett. 24 (14) (1997) 1731–1734.
[4] E.A. Gerken, U.S. Inan, C.P. Barrington-Leigh, Telescopic imaging of sprites, Geophys. Res. Lett. 27 (17) (2000) 2637–2640.
[5] E.A. Gerken, U.S. Inan, A survey of streamer and diffuse glow dynamics observed in sprites using telescopic imagery, J. Geophys. Res. – Space Phys. 107 (A11) (2002) 1344:12.
[6] E.A. Gerken, U.S. Inan, Observations of decameter-scale morphologies in sprites,J. Atmos. Solar–Terr. Phys. 65 (5) (2003) 567–572.
[7] V.P. Pasko, U.S. Inan, T.F. Bell, Spatial structure of sprites, Geophys. Res. Lett. 25 (12) (1998) 2123–2126.
[8] V.P. Pasko, H.C. Stenbaek-Nielsen, Diffuse and streamer regions of sprites, Geophys. Res. Lett. 29 (10) (2002) 1440:4.
[9] Y.P. Raizer, G.M. Milikh, M.N. Shneider, S.V. Novakovski, Long streamers in the upper atmosphere above thundercloud, J. Phys. D – Appl. Phys. 31 (22) (1998) 3255–3264.
[10] Y.P. Raizer, Gas Discharge Physics, Springer-Verlag, Berlin, Heidelberg, 1991.
[11] G.D. Moss, V. Pasko, N. Liu, G. Veronis, Monte Carlo model for analysis of thermal runaway electrons in streamer tips in transient luminous events and streamer zones of lightning leader, J. Geophys. Res. 111 (2006) A011350.
[12] D.M. Smith, L.I. Lopez, R.P. Lin, C.P. Barrigton-Leigh, Terrestrial gamma-ray flashes observed up to 20 meV, Science 307 (5712) (2005) 1085–1088.
[13] C.B. Moore, K.B. Eack, G.D. Aulich, W. Rison, Energetic radiation associated with lightning stepped-leaders, Geophys. Res. Lett. 28 (11) (2001) 2141–2144.
[14] G.K. Parks, B.H. Mauk, R. Spiger, J. Chin, X-ray enhancements detected during thunderstorm and lightning activities, Geophys. Res. Lett. 8 (1981) 1176–1179.
[15] J.R. Dwyer, H.K. Rassoul, Z. Saleh, M.K. Uman, J. Jerauld, J.A. Plumer, X-ray bursts produced by laboratory sparks in air, Geophys. Res. Lett. 32 (2005) L20809.
[16] N.Y. Liu, V.P. Pasko, Effects of photoionization on propagation and branching of positive and negative streamers in sprites, J. Geophys. Res. – Space Phys. 109 (A4) (2004) A04301:17.

[17] K. Nanbu, Probability theory of electron–molecule, ion–molecule, molecule–molecule, and coulomb collisions for particle modelling of materials processing plasmas and gases, IEEE Trans. Plasma Sci. 28 (3) (2000) 971–990.
[18] C.K. Birdsall, Particle in cell charged particle simulations, plus Monte Carlo collisions with neutral atoms, IEEE Trans. Plasma Sci. 19 (2) (1991) 65–85.
[19] C.K. Birdsall, A.B. Langdon, Plasma Physics via Computer Simulation, McGraw-Hill Book Company, 1985.
[20] K. Nanbu, Simple method to determine collisional event in Monte Carlo electron–molecule collision, Jpn. J. Appl. Phys. 33 (8) (1994) 4752–4753.
[21] V. Vahedi, M. Surendra, A Monte Carlo collision model for the particle in cell method: applications to argon and oxygen discharges, Comput. Phys. Commun. 87 (1995) 179–198.
[22] C.B. Opal, W.K. Peterson, E.C. Beaty, Measurements of secondary-electron spectra produced by electron impact ionization of a number of simple gases, J. Chem. Phys. 55 (8) (1997) 4100–4106.
[23] J.P. Boeuf, L.C. Pitchord, W.L. Morgan, Siglo cross sections database. <http://www.siglo-kinema.com/>.
[24] J.W. Liu, Total cross sections for high-energy electron scattering by h_2 ($^1\sigma_g^+$), n_2 ($^1\sigma_g^+$), and o_2 ($^3\sigma_g^-$), Phys. Rev. A 35 (2) (1987) 591–597.
[25] M. Inokuti, Inelastic collisions of fast charged particles with atoms and molecules – Bethe theory revisited, Rev. Mod. Phys. 43 (1971) 297–347.
[26] A. Okhrimovskyy, A. Bogaerts, R. Gijbels, Electron anisotropic scattering in gases: a formula for Monte Carlo simulations, Phys. Rev. E 65 (2002) 037402.
[27] A.V. Phelps, L.C. Pitchford, Anisotropic scattering of electrons by n_2 and its effect on electron transport, Phys. Rev. A 31 (5) (1985) 2932–2949.
[28] M.B. Zheleznyak, A.K. Mnatsakanyan, S.V. Sizykh, Photoionization of nitrogen and oxygen mixtures by radiation from a gas discharge, High Temp. 20 (1982) 357–362.
[29] E. Anderson, Z. Bai, C. Bischof, S. Blackford, J. Demmel, J. Dongarra, J. Ducroz, S. Greenbaum, A. Hammaring, A. McKenney, D. Sorensen, LAPACK Users' Guide, 3rd ed., SIAM Publication, Philadelphia, 1999.
[30] J.P. Verboncoeur, Symmetric spline weighting for charge and current density in particle simulation, J. Comput. Phys. 174 (2001) 421–427.
[31] E.E. Kunhardt, Y. Tzeng, Development of an electron avalanche and its transition into streamers, Phys. Rev. A 38 (3) (1988) 1410–1421.
[32] C. Li, U. Ebert, W.J.M. Brok, Avalanche to streamer transition in particle simulations, IEEE Trans. Plasma Sci., in press.
[33] L.C. Pitchford, S.V. Oneil, J.R. Rumble, Extended Boltzmann analysis of electron swarm experiments, Phys. Rev. A 23 (1) (1981) 294–304.
[34] A.A. Kulikovsky, The role of photoionization in positive streamer dynamics, J. Phys. D – Appl. Phys. 33 (2000) 1514–1524.
[35] A. Bourdon, V.P. Pasko, N.Y. Liu, S. Celestin, P. Segur, E. Marode, Efficient models for photoionization produced by non-thermal gas, Plasma Sources Sci. Technol. 16 (2007) 656–678.
[36] C. Li, W. Brok, U. Ebert, J.J. van der Mullen, Deviations from the local field approximation in negative streamer heads, J. Appl. Phys. 101 (123305) (2007).
[37] C. Montijn, W. Hundsdorfer, U. Ebert, An adaptive grid refinement strategy for the simulation of negative streamers, J. Comput. Phys. 219 (2006) 801–835.
[38] R. Roussel-Dupre, A.V. Gurevich, On runaway breakdown and upward propagating discharges, J. Geophys. Res. 101 (A2) (1996) 2297–2311.
[39] R. RousselDupre, A.V. Gurevich, On runaway breakdown and upward propagating discharges, J. Geophys. Res. – Space Phys. 101 (A2) (1996) 2297–2311.
[40] A.V. Gurevich, K.P. Zybin, Runaway breakdown and the mysteries of lightning, Phys. Today 58 (5) (2005) 37.
[41] G.J. Fishman, P.N. Bath, R. Mallozzi, J.M. Horack, T. Koshut, C. Kouveliotou, G.N. Pendleton, C.A. Meegan, R.B. Wilson, W.S. Paciesas, S.J. Goodman, H.J. Christian, Discovery of intense gamma-ray flashes of atmospheric origin, Science 264 (1994) 1313.
[42] L.P. Babich, E.N. Donskoy, K.F. Zelenskii, R.I. Il'kaev, I.M. Kutsyk, T.V. Loiko, R.A. Roussel-Dupre, Observation of the initial stage in the development of an avalanche of relativistic runaway electrons under normal atmospheric conditions, DOKLADY Phys. 47 (1) (2002) 1–4.
[43] J.R. Dwyer, H.K. Rassoul, M. Al-Dayeh, L. Caraway, A. Chrest, B. Wright, E. Kozak, J. Jerauld, M.A. Uman, V.A. Rakov, D.M. Jordan, K.J. Rambo, X-ray bursts associated with leader steps in cloud-to-ground lightning, Geophys. Res. Lett. 32 (2005) L01803.
[44] J.R. Dwyer, M.A. Uman, H.K. Rassoul, M. Al-Dayeh, L. Caraway, J. Jerauld, V.A. Rakov, D.M. Jordan, K.J. Rambo, V. Corbin, B. Wright, Energetic radiation produced during rocket-triggered lightning, Science 299 (2003) 694–697.
[45] J.R. Dwyer, H.K. Rassoul, M. Al-Dayeh, L. Caraway, B. Wright, A. Chrest, M.A. Uman, V.A. Rakov, K.J. Rambo, D.M. Jordan, J. Jerauld, C. Smyth, Measurements of X-ray emission from rocket-triggered lightning, Geophys. Res. Lett. 31 (2004) L05118, doi:10.1029/2003GL018770.
[46] J.R. Dwyer, H.K. Rassoul, M. Al-Dayeh, L. Caraway, B. Wright, A. Chrest, M.A. Uman, V.A. Rakov, K.J. Rambo, D.M. Jordan, J. Jerauld, C. Smyth, A ground level γ-ray burst observed in association with rocket-triggered lightning, Geophys. Res. Lett. 31 (2004) L05119, doi:10.1029/2003GL018771.
[47] L.P. Babich, A new type of ionization wave and the mechanism of polarization self-acceleration of electrons in gas discharges at high overvoltages, Sov. Phys. Dokl. 263 (1982) 7679.
[48] N.Y. Liu, V.P. Pasko, Effects of photoionization on similarity properties of streamers at various pressures in air, J. Phys. D – Appl. Phys. 39 (2006) 327–334.

[49] G.V. Naidis, On photoionization produced by discharges in air, Plasma Sources Sci. Technol. 15 (2006) 253–255.
[50] A. Luque, U. Ebert, C. Montijn, W. Hundsdorfer, Photoionisation in negative streamers: fast computations and two propagation modes, Appl. Phys. Lett. 90 (2007) 081501.
[51] A.A. Kulikovsky, The role of absorption length of photoionizing radiation in streamer dynamics in weak fields: a characteristic scale of ionization domain, J. Phys. D: Appl. Phys., Rapid Commun. 33 (2000) L5–L7.
[52] N. Liu, V.P. Pasko, D.H. Burkhardt, H.U. Frey, S.B. Mende, H.T. Su, A.B. Chen, R.R. Hsu, L.C. Lee, H. Fukunishi, Y. Takahashi, Comparison of results from sprite streamer modeling with spectrophotometric measurements by ISUAL instrument on FORMOSAT-2 satellite, Geophys. Res. Lett. 33 (2006) L01101.
[53] C.L. Kuo, R.R. Hsu, H.T. Su, A.B. Chen, L.C. Lee, S.B. Mende, H.U. Frey, H. Fukunishi, Y. Takahashi, Electric fields and electron energies inferred from the ISUAL recorded sprites, Geophys. Res. Lett. 32 (2005) L19103.
[54] A.V. Gurevich, P.N. Lebedev, G.M. Milikh, R. Roussel-Dupre, Runaway electron mechanism of air breakdown and preconditioning during a thunderstorm, Phys. Rev. A 165 (1992) 463–468.